Simplified Analysis of PWM Converters Using Model of PWM Switch Part II: Discontinuous Conduction Mode

VATCHÉ VORPÉRIAN
Virginia Polytechnic Institute and State University

According to the method of state-space averaging, when a pulsewidth modulation (PWM) converter enters discontinuous conduction mode, the inductor current state is lost from the average model of the converter. In this work, it is shown that there is neither theoretical nor experimental justification of the disappearance of the inductor state as claimed by the method of state-space averaging. For example, when the model of the PWM switch in discontinuous conduction mode (DCM) is substituted in the buck, boost, or buck-boost converter while the inductor is left intact, the average model has two poles. The first pole f_{p1} agrees with the single pole of state-space averaging, while the second pole f_{p2} occurs in the range $f_{p2} \geq F_s/\pi$. It is also shown that the right-half plane zeros in the control-to-output transfer functions of the boost, buck-boost and Cuk converters in continuous conduction mode are also present in discontinuous conduction mode as well.

Manuscript received February 16, 1989; revised June 16, 1989.

IEEE Log No. 33463B.

Author's address: Virginia Power Electronics Center, Dep't. of Electrical Engineering, Virginia Polytechnic Institute and State University, Blacksburg, VA 24061.

INTRODUCTION

In this article the model of the pulsewidth modulation (PWM) switch in discontinuous conduction mode (DCM) is developed and used in the analysis of PWM converters operating in DCM. As in the case of continuous conduction mode (CCM) [3], the model of the PWM switch in DCM represents the dc and small-signal characteristics of the nonlinear part of the converter which consists of the active and passive switch pair as shown in Fig. 1. In contrast to the model in CCM, the model of the PWM switch in DCM contains small-signal resistances which damp the low-pass filter to the point where two real poles are formed. The physical significance of these small-signal resistances is easy to understand as they represent the load dependent nature of the conversion ratio of these converters in DCM. The motivation and advantages behind the method of analysis presented here are discussed in Part I of this paper [3].

Whereas, use of the model of the PWM switch in CCM yields the *same* results as those given by the method of state-space averaging, in DCM the model of the PWM switch yields results which are *different* than those given by state-space averaging [1]. The fundamental difference between the two methods is that state-space averaging predicts that the discontinuous current state does not contribute to the order of the average model while the PWM switch model predicts otherwise.

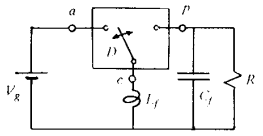

Fig. 1. PWM switch in "common-common" configuration.

Prior to the development of the methods of analysis known today, power supply designers observed the *transient* response of power supplies in continuous and discontinuous conduction mode. For the buck, boost, and buck-boost converters operating in CCM, the transient response was clearly seen to be second order. In DCM, however, the transient response of these converters seemed to be first order. The methods of analysis that were developed later, namely the method of state-space averaging [1], literally were constrained to yield results that would corroborate the observed first-order transient response. The *phase* response in a simple frequency-response measurement (up to one-half the switching frequency), however, *clearly* shows that the system is still a second-order system. The model of the PWM switch in DCM explains these results in a very simple and succinct way. When the model of the PWM switch in DCM is substituted in the converter while the inductor is left intact, the system has two real poles. The first

pole f_{p1} is the same as that given by state-space averaging, while the second pole f_{p2} occurs in the range $f_{p2} \geq F_s/\pi$. The contribution of the second pole on the phase response can be significant and easily verifiable in the frequency range below one-half the switching frequency. Furthermore, since the second pole corresponds to a time constant shorter than half the switching period, its contribution to the transient response will decay in one switching period or less, and hence the observed transient response will be dominated by the first pole.

The purpose of this article is two fold: first, to present a simple and circuit-oriented approach to the analysis of converters in DCM, and second, to show that there is simply neither theoretical nor experimental justification to the disappearance of the discontinuous current state from the average model as previously believed and later advocated by the method of state-space averaging [1].

DC AND SMALL-SIGNAL MODEL OF PWM SWITCH IN DCM

As in the case of the model of the PWM switch in CCM [3], the relationship between the average and instantaneous terminal voltages remains invariant no matter which converter the PWM switch is implemented in. Fig. 1 shows the buck-boost converter operating in DCM which corresponds to the PWM switch in the "common-common" configuration. In Part I, we considered the model of the PWM switch in CCM in the "common-passive" configuration which corresponds to the buck converter. The terminal voltages and currents of the PWM switch are defined in Fig. 2 and the instantaneous terminal currents are shown in Fig. 3. According to Fig. 3, the following expressions for the average terminal currents and voltages can be easily verified

$$i_a = \frac{i_{pk}}{2} d \tag{1}$$

$$i_p = \frac{i_{pk}}{2} d_2 \tag{2}$$

$$v_{ac} = L \frac{i_{pk}}{dT_s} \tag{3}$$

$$v_{cp} = L \frac{i_{pk}}{d_2 T_s}. \tag{4}$$

From these equations the following relationships between the average terminal voltages and currents can be deduced:

$$i_a = \frac{d}{d_2} i_p \tag{5}$$

$$v_{ac} = \frac{d_2}{d} v_{cp} \tag{6}$$

$$d_2 = \frac{2LF_s}{d} \frac{i_a}{v_{cp}} = \frac{2LF_s}{d} \frac{i_p}{v_{ac}}. \tag{7}$$

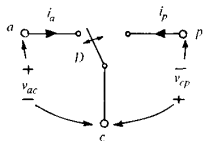

Fig. 2. Voltages and currents of PWM switch.

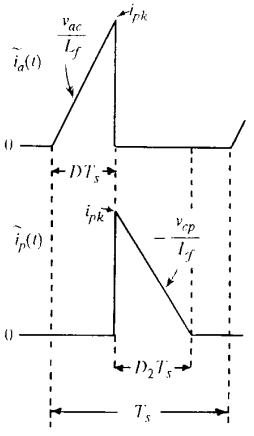

Fig. 3. Terminal currents of PWM switch in DCM.

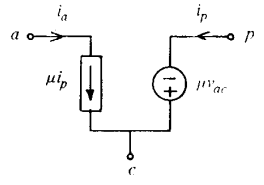

Fig. 4. Average model of PWM switch in DCM.

The average model follows from (5)–(7) as shown in Fig. 4 where

$$v_{cp} = \mu v_{ac} \tag{8a}$$

$$i_a = \mu i_p \tag{8b}$$

$$\mu = \frac{d^2}{2LF_s} \frac{v_{cp}}{i_a} = \frac{d^2}{2LF_s} \frac{v_{ac}}{i_p}. \tag{8c}$$

When the average model is used in the dc analysis of PWM converters in DCM, the quantities in (8) are replaced by their dc values, i.e., D, V_{pc}, I_a, etc.

The small-signal model is obtained from the relationship among the perturbation in average terminal quantities at a given dc operating point (I_p, V_{ac}, D). Hence, perturbation of (5) and (7) results in (after some algebra)

$$\hat{i}_a = \hat{v}_{ac} g_i + k_i \hat{d} \tag{9a}$$

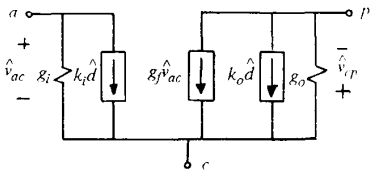

Fig. 5. Small-signal model of PWM switch in DCM.

where

$$g_i = \frac{I_a}{V_{ac}} \tag{9b}$$

$$k_i = \frac{2I_a}{D}. \tag{9c}$$

Perturbation of (6) and (7) results in

$$\hat{i}_p = g_f \hat{v}_{ac} + k_0 \hat{d} - g_0 \hat{v}_{cp} \tag{10a}$$

where

$$k_0 = \frac{2I_p}{D} \tag{10b}$$

$$g_0 = \frac{I_p}{V_{cp}} \tag{10c}$$

$$g_f = \frac{2I_p}{V_{ac}}. \tag{10d}$$

Equations (9a) and (10a) correspond to the equivalent circuit model shown in Fig. 5.

ANALYSIS OF PWM CONVERTERS USING MODEL OF PWM SWITCH IN DCM

In this section the model of the PWM switch in DCM is used to analyze the buck, boost, buck-boost, and Cuk converters in DCM. The buck and Cuk converters are analyzed in detail and their experimental and predicted results are compared. Whereas, the buck, boost, and buck-boost converters have been analyzed previously for dc and small-signal characteristics using the method of state-space averaging [1], the Cuk converter has been analyzed only for dc characteristics while its small-signal characteristics have been determined only experimentally [2]. Perhaps, the lack of analysis of the Cuk converter in DCM is due to the complicated method of state-space averaging as mentioned in [2]. Hence, once again, in order to fully appreciate the model of the PWM switch, one should go through the analysis of the Cuk converter in DCM using the method of state-space averaging outlined in [1], which to the best of the author's knowledge has not been done, and compare it with the method given here using the model of the PWM switch. Furthermore, it should be more satisfying to use the simple model of the PWM switch and obtain more accurate results than to use the more complex method of state-space averaging and obtain less accurate results.

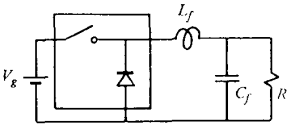

Fig. 6. Buck converter.

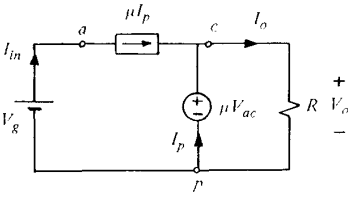

Fig. 7. Buck converter to be analyzed for dc characteristics in DCM.

Buck Converter in DCM

The buck converter shown in Fig. 6 is analyzed for dc characteristics, line-to-output, and control-to-output transfer functions.

DC Analysis: Under dc conditions, point-by-point substitution of the average PWM switch model of Fig. 4 in the buck converter results in the circuit in Fig. 7 from which we get

$$V_0 = \mu V_{ac} = \mu(V_g - V_0) \tag{11}$$

which gives

$$M = \frac{V_0}{V_g} = \frac{1}{1 + 1/\mu}. \tag{12}$$

Next, the amplification factor μ of the switch is determined in terms of the converter quantities as follows:

$$\mu = \frac{D^2}{2LF_s}\frac{V_{cp}}{I_a} = \frac{D^2}{2LF_s}\frac{V_0}{I_{in}} = \frac{D^2}{KM} \tag{13}$$

where

$$M = \frac{I_{in}}{I_0}; \qquad K = \frac{2LF_s}{R}. \tag{14}$$

Substitution of (13) in (12) gives

$$M = \frac{1}{1 + \dfrac{KM}{D^2}} \tag{15}$$

which is a quadratic equation in M the root of which is given by

$$M = \frac{2}{1 + \sqrt{1 + 4K/D^2}}. \tag{16}$$

The critical value of K which determines the boundary between DCM and CCM can be obtained from (15) by letting $M = D$, which is the value of M in CCM, and obtain

$$K_{\text{crit}} = 1 - D. \tag{17}$$

This completes the dc analysis of the buck in DCM.

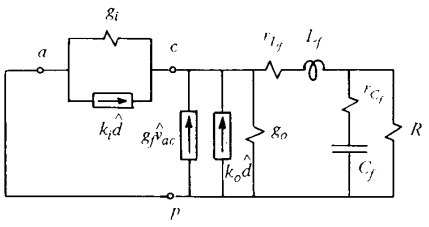

Fig. 8. Buck converter to be analyzed for control-to-output transfer function in DCM.

Control-to-Output Transfer Function: To perform this analysis, we substitute the model of the PWM switch in DCM in the buck converter and we short V_g as shown in Fig. 8. The small-signal current source $g_f\hat{v}_{ac}$ connected between terminals a and c acts like a conductance g_f as can be easily verified. Hence, the three conductances g_0, g_i, and g_f can be combined into a single conductance while the two controlled current sources can be combined in a single current source as shown in Fig. 9 where

$$r = \frac{1}{g_i + g_0 + g_f} \tag{18a}$$

$$k_d = k_i + k_0. \tag{18b}$$

Next, we evaluate the small-signal parameters at the dc operating point using (9) and (10) as follows:

$$k_i + k_0 = \frac{2}{D}(I_a + I_p) = \frac{2I_0}{D}. \tag{19}$$

Likewise, for r we obtain after a *few* lines of algebra and assuming r_{L_f} is negligible in the dc analysis:

$$r = \frac{1}{g_i + g_0 + g_f} = R(1 - M). \tag{20}$$

The control-to-output transfer function can be obtained from Fig. 9

$$\frac{\hat{v}_0}{\hat{d}} = H_d \frac{1 + s/s_{z1}}{1 + a_1 s + a_2 s^2} \tag{21}$$

where

$$H_d = \frac{2I_0}{D}\frac{rR}{r + R + r_{L_f}} \tag{22a}$$

$$s_{z1} = \frac{1}{r_{C_f} C_f} \tag{22b}$$

$$a_1 = \frac{L}{r_{L_f} + r + R} + C_f[r_{C_f} + R\|(r + r_{L_f})] \tag{22c}$$

$$a_2 = LC_f \frac{r_{C_f} + R}{r_{L_f} + r + R}. \tag{22d}$$

Although at this point the control-to-output transfer function is completely determined, we should perform some analytical simplifications in order to see if familiar results known from state-space averaging [1] are present in (22). To do so, we rewrite a_1 assuming

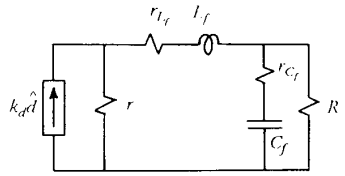

Fig. 9. Simplification of circuit in Fig. 8.

$r_{C_f} = r_{L_f} = 0$ and obtain

$$a_1 = C_f R \frac{1 - M}{2 - M}\left[1 + \frac{1}{RC_f}\frac{L}{R}\frac{1}{1 - M}\right].$$

The second term in the brackets can be shown to be much less than unity by writing it as follows

$$\frac{1}{RC_f}\frac{L}{R}\frac{1}{1 - M} = \frac{T_s}{2RC_f}\frac{K}{1 - M}. \tag{23}$$

But, from (15) we have

$$\frac{1 - M}{K} = \left(\frac{M}{D}\right)^2 \tag{24}$$

so that (23) can be written as

$$\frac{T_s}{2RC_f}\left(\frac{D}{M}\right)^2 \ll 1. \tag{25}$$

The above inequality is true because of two reasons. First, the switching time is much shorter than the output filter time constant and second, $D < M$ because the conversion ratio in CCM (D) is less than the conversion ratio in DCM for a given D. Hence, we have

$$a_1 \simeq RC_f \frac{1 - M}{2 - M}. \tag{26}$$

Using the inequality in (25), we can show that

$$a_1 \gg \frac{a_2}{a_1}$$

so that the quadratic can be factored as

$$\frac{\hat{v}_0}{\hat{d}} = H_d \frac{1 + s/s_{z1}}{(1 + s/s_{p1})(1 + s/s_{p2})} \tag{27}$$

where

$$s_{p1} = \frac{1}{a_1} = \frac{1}{RC}\frac{2 - M}{1 - M} \tag{27a}$$

$$s_{p2} = \frac{a_1}{a_2} = 2F_s\left(\frac{M}{D}\right)^2. \tag{27b}$$

It can be seen now that the dominant pole is given by (27a) which is the same as the single pole given by state averaging [1]. There is a second pole, however, which satisfies the following general inequality:

$$f_{p2} = \frac{s_{p2}}{2\pi} \geq \frac{F_s}{\pi}\ \text{Hz} \tag{27c}$$

which can be easily verified from (27b), as explained earlier, by noting that the conversion ratio M in DCM is always larger than the conversion ratio in CCM,

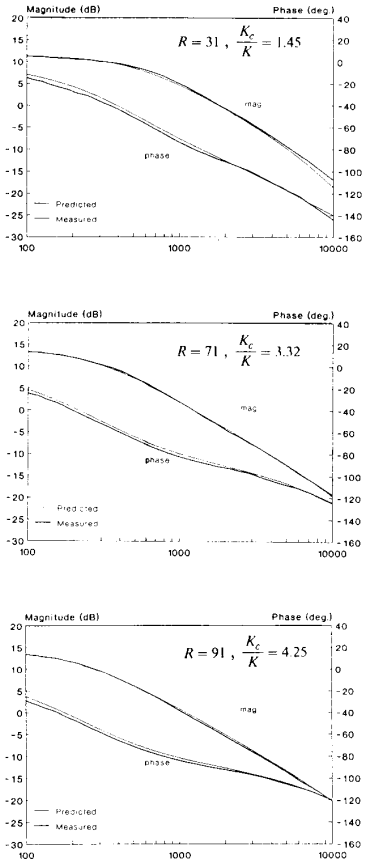

Fig. 10. Experimental and predicted control-to-output transfer function of buck converter for 3 cases of DCM.

which for the buck converter is given by D. The second pole starts at F_s/π Hz when the converter is operating at the boundary between DCM and CCM and begins to move outwards as the converter enters deeper into DCM. This result is general and is common to the buck, boost, buck-boost, and Cuk converters. It is clear then why the contribution of this pole to the magnitude response is hardly noticeable but to the phase response it is quite noticeable.

A buck converter was built with the following circuit parameters: $L_f = 380\ \mu$H, $C_f = 29\ \mu$F, $r_{L_f} = 0.12\Omega$, $D = 0.24$, $F_s = 20$ KHz, and $R = 31$, 71, 91Ω. (The zero owing to the ESR of the output filter capacitor was in the range of a few hundred kilohertz because the capacitor consisted of ten multilayer ceramic capacitors in parallel which have negligible ESR.) The experimental and predicted results are shown in Fig. 10 for three different cases as the converter enters deeper into DCM, i.e., $R = 31$, 71, 91Ω. The phase response clearly shows that the converter in DCM is still a second-order system and not a first-order system as assumed in [1].

Open-Loop Line-to-Output Transfer Function: To perform this analysis, we replace V_g with a

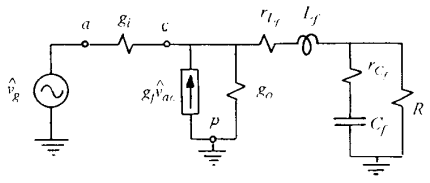

Fig. 11. Analysis of buck converter for line-to-output transfer function in DCM.

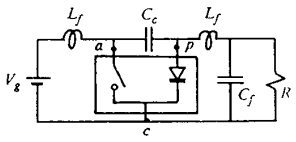

Fig. 12. Cuk converter.

small-signal perturbation $\hat{v}_g$ and remove the duty-ratio controlled sources $k_i d$ and $k_0 d$ from the model of PWM switch as shown in Fig. 11. The line-to-output transfer function has exactly the same form as the control-to-output transfer function in (21) except that the low-frequency asymptote is given by M:

$$\frac{\hat{v}_0}{\hat{v}_g} = M\frac{1 + s/s_{z1}}{1 + a_1 s + a_2 s^2} \tag{28}$$

where M, s_{z1}, a_1, and a_2 are given in (16) and (22b)–(22d).

Cuk Converter in DCM

In this section, the Cuk converter shown in Fig. 12 is analyzed for dc characteristics, control-to-output, and line-to-output transfer functions. The dc characteristics of this converter in DCM are analyzed in detail in [2], but its small-signal characteristics are determined only experimentally in [2].

Two things are shown here. First, using the model of the PWM switch one can determine the small-signal characteristics as easily as the dc characteristics. Second, the small-signal transfer functions predicted in this section agree very well with the experimental results given in [2] and confirm the fact that the Cuk converter in DCM is a *fourth-order* system and *not* a third-order system (because of the disappearance of the sum of the inductor current states as claimed in [2].)

DC Analysis: As in the case of the buck converter, point-by-point substitution of the model of the PWM switch in the Cuk converter results in the circuit of Fig. 13 from which we get

$$V_0 = \mu V_{ac} = \mu V_g \rightarrow M = \mu. \tag{29}$$

The amplification factor μ is determined next in terms of the converter quantities as follows:

$$\mu = \frac{D^2}{2L_1 \| L_2 F_s}\frac{V_{ac}}{I_p} = \frac{D^2}{KM} \tag{30}$$

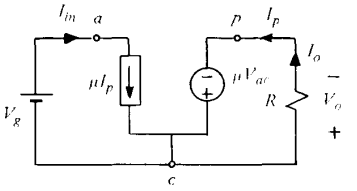

Fig. 13. Cuk converter to be analyzed for dc characteristics.

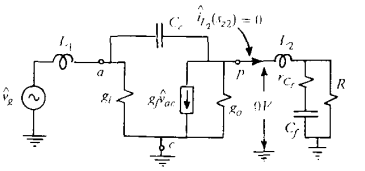

Fig. 14. Cuk converter to be analyzed for line-to-output transfer function. Null conditions for determination of zero due to filter current is indicated.

where we have made use of the fact that $V_{ac} = V_g$, $I_p = V_0/R$. Also, when writing $L_1||L_2$ we have used the fact that the current through the active and passive terminals is determined by the sum of the currents in L_1 and L_2. Substitution of (30) in (29) results in a quadratic equation in M

$$M^2 - \frac{D^2}{K} = 0 \tag{31}$$

which gives

$$M = \frac{D}{\sqrt{K}}. \tag{32}$$

The critical value of K which determines the boundary between CCM and DCM is obtained by letting $M = D/D'$, which is the conversion ratio of the Cuk converter in CCM, in (31):

$$K_c = D'^2. \tag{33}$$

This completes the analysis of the dc characteristics of the Cuk converter in DCM.

Open-Loop Line-to-Output Transfer Function: Point-by-point substitution of the model of the PWM switch in DCM in the Cuk converter results in the circuit of Fig. 14. The duty-ratio controlled sources are removed for the purpose of determining the open-loop line-to-output transfer function. The expected form of the line-to-output transfer function is of the form

$$\frac{\hat{v}_0}{\hat{v}_g} = M\frac{N(s)}{D(s)} \tag{34}$$

where

$$D(s) = 1 + a_1 s + a_2 s^2 + a_3 s^3 + a_4 s^4$$

and $N(s)$ and $D(s)$ are to be determined. Before proceeding, the small-signal parameters are evaluated at the operating point as follows:

$$g_i = \frac{I_a}{V_{ac}} = \frac{I_{in}}{V_g} = \frac{M^2}{R} \tag{35a}$$

$$g_f = \frac{2I_p}{V_{ac}} = \frac{2I_0}{V_g} = \frac{2M}{R} \tag{35b}$$

$$g_0 = \frac{I_p}{V_{pc}} = \frac{I_0}{V_0} = \frac{1}{R}. \tag{35c}$$

As explained in Part I of this paper [3], we can use certain network tricks to determine the numerator and denominator of a transfer function. These methods are also discussed in [4]. I will only discuss here the determination of the zeros of (34) which correspond to the *nulls* of the transform output voltage and transform filter current. The first null of the transform output voltage is clearly given by the null of the impedance across it. Hence, one of the nulls is simply given by the zero due to the ESR of the output filter capacitor:

$$r_{C_f} + \frac{1}{sC_f}\bigg|_{s=-s_{z1}} = 0 \rightarrow s_{z1} = \frac{1}{r_{C_f}C_f}. \tag{36}$$

The condition of the second zero is given by the null in the filter current $i_{L_2}(s_{z2}) = 0$ as shown in Fig. 14. The conditions of this second null imply

$$\hat{i}_{C_c} = g_f \hat{v}_{ac} \rightarrow \hat{v}_{ac} s_{z2} C_c = g_f \hat{v}_{ac}$$

which gives a right-half plane zero

$$s_{z2} = \frac{g_f}{C_c} = \frac{2M}{RC_c} \tag{37}$$

where we have made use of (35b). Hence the numerator in (34) is given by

$$N(s) = (1 + s/s_{z1})(1 - s/s_{z2}). \tag{38}$$

In order to determine the coefficients a_i in the denominator, one can use the method of time constants as explained in [4]. I only give the results here (assuming negligible parasitics) and show how the fourth-order denominator can be factored approximately in analytical form and gain valuable insight into the dynamics of the converter. The denominator in factored form is given by

$$D(s) = \left(1 + \frac{s}{s_{p1}}\right)\left(1 + \frac{s}{s_{p2}}\right)(1 + s/\omega_0 Q + s^2/\omega_0^2) \tag{39}$$

where

$$s_{p1} = \frac{2}{R(C_c + C_f)} \tag{40a}$$

$$s_{p2} = 2F_s\left[\frac{1/D}{1 + 1/M}\right]^2 > 2F_s \tag{40b}$$

$$\omega_0 = \frac{1}{\sqrt{C_e(L_1 + L_2)}} \tag{40c}$$

$$\frac{1}{Q} = \frac{1}{Q_1}\frac{C_e}{C'} + \frac{1}{Q_2} - \left(\frac{s_{p1}}{\omega_0} + \frac{\omega_0}{s_{p2}}\right) \tag{40d}$$

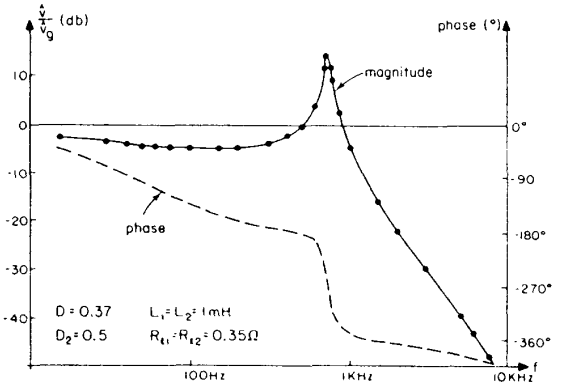

Fig. 15. Experimentally determined line-to-output transfer function of Cuk converter in DCM as given in [2].

where

$$C_e = C_c \| C_f = \frac{C_c C_f}{C_c + C_f} \tag{40e}$$

$$C' = \frac{C_f}{1+(1+M)^2} \Bigg\| \frac{C_c}{M^2} \tag{40f}$$

$$Q_1 = \frac{R}{\omega_0 L_1}; \qquad Q_2 = \frac{R}{\omega_0 L_2}. \tag{40g}$$

It can be seen that in addition to the dominant pole s_{p1}, there is a second real pole s_{p2} which has the general behavior as explained in (27c). The frequency of the quadratic term ω_0 lies between the two real poles. The fact that $1/Q$ is equal to the difference of two factors accounts for the high Q typically observed with the Cuk converter.

The experimental Cuk converter discussed in [2] has the following circuit parameters: $C_f = C_c = 47\mu$F, $L_1 = L_2 = 1$ mH, $D = 0.37$, $F_s = 20$ KHz, and $R = 75\Omega$. The following components of the line-to-output transfer function are computed: $M = 0.77$, $f_{z2} = 69$ Hz (right-half-plane zero), $f_{p1} = 45$ Hz, $f_{p2} = 8.79$ KHz, $f_0 = \omega_0/2\pi = 734$ Hz, and $Q = 16$.

The experimentally determined line-to-output transfer function reported in [2, Fig. (26)] is shown here in Fig. 15. The predicted results using the model of the PWM switch in DCM given in (34), (38), (39) are shown in Fig. 16. The remarkably good agreement between the experimental and predicted results leaves no doubt that the Cuk converter in DCM is a *fourth-order* system and not a third-order system as claimed in [2]. In particular, the reader should see that the phase shift in excess of 360 degrees is clearly indicative of the system being fourth-order with a right-half-plane zero.

Control-to-Output Transfer Function: The model of the PWM switch in DCM is substituted in the Cuk converter and V_g is shorted as shown in Fig. 17. The control-to-output transfer function is expected to be of

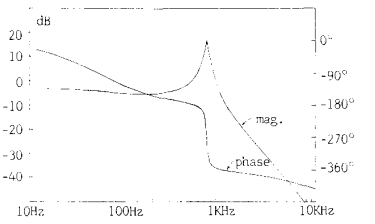

Fig. 16. Predicted line-to-output transfer function of Cuk converter in DCM using model of PWM switch in DCM. Agreement with Fig. 15 is very good.

the form

$$\frac{\hat{v}_0}{\hat{d}} = H_d \frac{C(s)}{D(s)} \tag{41}$$

where

$$H_d = V_g \frac{dM}{dD} = \frac{V_g}{\sqrt{K}} \tag{42}$$

and $D(s)$ is exactly the same as in (39) and (40). Therefore, all we need to determine is the numerator $C(s)$ in (41). As discussed earlier, the numerator of a transfer function corresponds to the null conditions of a transfer function which for the Cuk converter are shown in Fig. 17. The first null condition due to the ESR of the output filter capacitor is the same as in the case of the line-to-output transfer function and is given by (36). The second null condition is given by the current in the output filter inductor as shown in Fig. 17 which for $i_{L_2}(s) = 0$ shows

$$\hat{v}_{ac} = \frac{1}{sC_c}(g_f \hat{v}_{ac} + k_0 \hat{d}) \tag{42a}$$

which gives

$$\hat{v}_{ac} = \frac{k_0 \hat{d}}{-g_f + sC_c}. \tag{42b}$$

Also, we have

$$g_f \hat{v}_{ac} + k_0 \hat{d} = -k_i \hat{d} - \frac{1}{\frac{1}{g_i} \| sL_1} \frac{g_f \hat{v}_{ac} + k_0 \hat{d}}{sC_c}. \tag{43}$$

Substitution of (42b) in (43) yields a quadratic

$$s^2 L_1 C_c \left(1 + \frac{k_i}{k_0}\right) + sL_1 \left(g_i - \frac{k_i}{k_0} g_f\right) + 1 = 0. \tag{44a}$$

Finally, substitution of the small-signal parameters evaluated at the operating point given in (35) gives the numerator $C(s)$

$$C(s) = \left(1 + \frac{s}{s_{z1}}\right)\left(1 - \frac{s}{\omega_a Q_a} + \frac{s^2}{\omega_a^2}\right) \tag{44b}$$

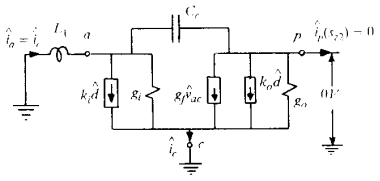

Fig. 17. Cuk converter to be analyzed for control-to-output transfer function in DCM. Null condition corresponding to zero due to filter current is shown.

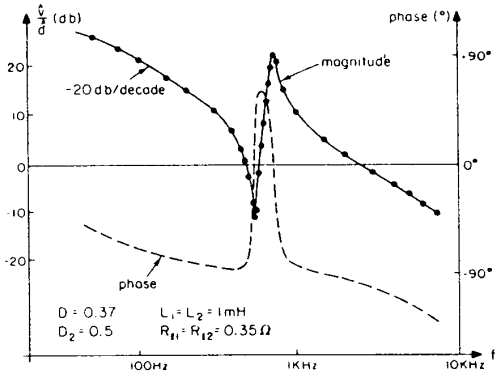

Fig. 18. Experimentally determined control-to-output transfer function of Cuk converter in DCM as given in [2].

where

$$\omega_a = \frac{1}{\sqrt{L_1 C_c (1+M)}} \tag{45a}$$

$$\frac{1}{Q_a} = \frac{\omega_a L_1 M^2}{R} \tag{45b}$$

$$s_{z1} = \frac{1}{r_{C_f} C_f}. \tag{45c}$$

The quadratic in the numerator corresponds to complex *right-half-plane* zeroes (and not left-half-plane zeros as believed in [2]). The experimentally determined control-to-output transfer function as reported in [2, Fig. (27)] is shown here in Fig. 18. The predicted results obtained are shown in Fig. 19. Once again, the good agreement between the experimental and predicted results confirms the validity of the switch model and the fact that the Cuk converter in DCM is still a fourth-order system. In particular, the reader should pay close attention to the drooping phase past the two sharp Q points. (Note: owing, to the high Q in the numerator and the denominator, the phase in the vicinity of ω_a and ω_0 goes through a very sharp drop of 360 degrees. This may cause the measuring instrument to flip the measurement and maintain the reading between 180 and -180 degrees, giving the impression that the complex zeros are in the left-half-plane (as was believed in [2]) as shown in Fig. 18. In order for the predicted phase response to look the same as the one in Fig. 18, the calculating routine was requested to maintain its phase in the range of 180 and -180 degrees.)

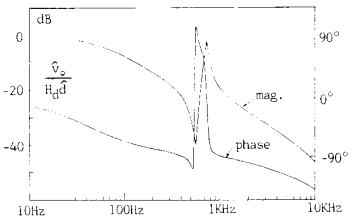

Fig. 19. Predicted control-to-output transfer function using model of PWM switch in DCM. Agreement with Fig. 18 is very good.

ZEROS OF CONTROL-TO-OUTPUT TRANSFER FUNCTION IN DCM

In addition to the widespread belief that the order of PWM converters in DCM is less than their order in CCM by one, there exists the myth that the right-half-plane zero in the control-to-output transfer function of the boost and buck-boost converters in CCM simply disappears in DCM. If we look at the complex right-half-plane zero of the Cuk converter in DCM given by (44), (45), we find that it has exactly the same dependence on the circuit parameters and M as does the complex right-half-plane zero in CCM. The complex right-half-plane zero of the Cuk converter in CCM is determined in [5] to be

$$\omega_a = \sqrt{\frac{D'}{L_1 C_c}} \tag{46a}$$

$$\frac{1}{Q_a} = \frac{D^2}{D'R}\sqrt{\frac{L_1}{D'C_c}}. \tag{46b}$$

Substitution of the conversion ratio $M = D/D'$ in (46a) and (46b) yields the same results given in (45b) and (45c). The same holds true for the right-half-plane zeros of the boost and buck-boost converters.

Boost Converter in DCM

The control-to-output transfer function of the boost converter in DCM can be shown to be given by

$$\frac{\hat{v}_0}{\hat{d}} = H_d \frac{(1+s/s_{z1})(1-s/s_{z2})}{(1+s/s_{p1})(1+s/s_{p2})} \tag{47}$$

where s_{z1} is the usual zero due to the output filter capacitor given in (36) and

$$s_{z2} = \frac{R}{M^2 L_f} \tag{48a}$$

$$s_{p1} = \frac{2M-1}{M-1}\frac{1}{RC_f} \tag{48b}$$

$$s_{p2} = 2F_s\left(\frac{1-1/M}{D}\right)^2 \geq 2F_s \tag{48c}$$

$$H_d = \frac{2V_0}{D}\frac{M-1}{2M-1}. \tag{48d}$$

We see that the right-half-plane zero has exactly the same dependence on the circuit parameters in DCM as in CCM because the right-half-plane zero in CCM is given by $s_{z2} = RD'^2/L_f$. The relative position of the right-half-plane zero to the second pole can be easily determined and is given by

$$s_{z2} = \frac{s_{p2}}{1-1/M} > 2F_s. \tag{49}$$

Hence, s_{z2} occurs always after the second pole since $M > 1$ for the boost converter.

Buck-Boost Converter in DCM

For the buck-boost converter the zeros and the poles of the control-to-output transfer function are given by

$$s_{z2} = \frac{R}{M(1+M)L_f} \tag{50a}$$

$$s_{p1} = \frac{2}{RC_f} \tag{50b}$$

$$s_{p2} = 2F_s\left(\frac{1/D}{1+1/M}\right)^2 \geq 2F_s \tag{50c}$$

$$H_d = \frac{V_g}{\sqrt{K}}. \tag{50d}$$

Again it can be easily seen that the right-half-plane zero has the same dependence on M and the circuit parameters as the right-half-plane zero in CCM. The relative position of s_{z2} to s_{p2} is given by

$$s_{z2} = s_{p2}(1+1/M) > 2F_s. \tag{51}$$

Hence, as in the case of the boost converter, s_{z2} occurs after s_{p2}.

CONCLUSIONS

The model of the PWM switch in DCM, developed here, provides a simple and circuit-oriented approach to the analysis of PWM converters in DCM. In contrast to the model of the PWM switch in CCM, the model in DCM contains small-signal resistances which damp the low-pass filter to the point where two real poles appear. The first pole coincides with the well-known pole of state-space averaging, whereas the second pole f_{p2} occurs in the range $f_{p2} \geq F_s/\pi$.

For the first time, it is shown that the transition from continuous to discontinuous conduction mode of operation is not accompanied by a reduction in the order of the average model of the converter. The average model in both cases is of the same order, the difference being only in the damping.

REFERENCES

[1] Cuk, S. (1977)
A general unified approach to modelling switching dc-to-dc converters in discontinuous conduction mode.
In *IEEE Power Electronics Specialists Conference Proceedings*, 1977.

[2] Cuk, S. (1978)
Discontinuous inductor current mode in the optimum topology switching converter.
In *IEEE Power Electronics Specialists Conference Proceedings*, 1978.

[3] Vorpérian, V. (1990)
Simplified analysis of PWM using the model of the PWM switch, Part I: continuous conduction mode.
IEEE Transactions on Aerospace and Electronic Systems, **AES-26**, 2 (Mar. 1990).

[4] Vorpérian, V.
Circuit-oriented analysis of PWM converters using the model of the PWM switch.
Available from the author upon request.

[5] Polivka, W., Chetty, P., and Middlebrook, R. (1980)
State-space average modelling of converters with parasitics and storage-time modulation.
In *IEEE Power Electronics Specialists Conference Proceedings*, 1980.

Vattché Vorpérian received his B.S. and M.S. degrees in electrical engineering from Northeastern University, Boston, MA, in 1976 and 1977, respectively. He received his Ph.D. from Caltech, Pasadena, CA, in 1984.

In 1977, he joined the Digital Equipment Corporation in Maynard, MA, where he worked for two years on the design of computer power supplies. In 1979, he joined the power electronics group at California Institute of Technology at Pasadena, CA. Vorpérian then joined the faculty of the Bradley Department of Electrical Engineering at Virginia Polytechnic Institute and State University where he currently is an Assistant Professor. His current research interests include modeling and an analysis of resonant converters.

Dr. Vorpérian has published 11 papers and is a member of Sigma Xi.